ICAS 2020 SHANG HAI
International Council of the Aeronautical Sciences
32nd Congress of the International Council of the Aeronautical Sciences
September 6-10, 2021
Pudong Shangri-La, Shanghai, China

COUPLED HEAT TRANSFER CHARACTERISTICS ON CHEMICALLY REACTING INTERFACE OF HIGH-SPEED AIRCRAFT CONSIDERING WALL INJECTION

Qi You[1], Xiaofeng Yang[1], Lei Zeng[1,*], Yewei Gui[1], Yanxia Du[1], Lei Liu[1] & Guangming Xiao[1]

[1]State Key Laboratory of Aerodynamics, China Aerodynamics Research and Development Center

Abstract

The wall injection phenomena widely exist in thermal protection systems of high-speed aircrafts. In this paper, the wall injection boundary condition was implemented in the CAPTER code. After verifying the boundary condition, it was applied to the coupling modeling of chemically reacting interface. The effects of different ablation chemical reactions and ablation reaction coefficients on aerodynamic heating environment and flow field were studied by using this coupling modeling. The results show that the ablation reaction coefficient has a great influence on the aerodynamic heating environment and the flow field, and the superposition of different ablation reactions will produce a comprehensive effect. Meanwhile, the heat transfer characteristics of the ablation reaction are also studied in this paper.

Keywords: aerodynamic heating environment, wall injection, coupling modeling, ablation

1. Introduction

When high-speed aircrafts fly in near space, high Mach number will cause chemical reactions such as dissociation and ionization of oxygen and nitrogen of high temperature air in the flow field, and internal energy modes of molecules and atoms will be excited in different degrees, that is, high-temperature real-gas effects. The thermal protective materials on the surface of aircrafts will produce catalytic effect on the chemical reaction of high-temperature gas. If the aerodynamic heating is severe, ablation will occur on the thermal protective materials on the surface of aircrafts. Various gases produced by ablation will inject into the flow field and react with the gas components in the flow field. The above aerodynamic phenomena can be collectively referred to as Chemical nonequilibrium effect of high temperature gas, which has a serious impact on the aerodynamic heating environment of aircrafts [1].

The ablation reaction of high-speed aircrafts includes the direct reaction of thermal protective materials with the surrounding air and the chemical reaction of ablation product components in the flow field. Ablation involves different kinds of phenomena, among which kinds of chemical reactions, pyrolysis, evaporation and sublimation have wall injection effect. The ablation products inject into the boundary layer, blocking the heat transfer to the wall, thickening the boundary layer and reducing the aerodynamic heating. This phenomenon is called thermal blockage effect [2]. If the effect of wall injection on aerodynamic heating is not considered, the prediction deviation of aerodynamic heating environment and hot redundancy will be caused. A survey by Reynier, P. showed that when Stardust reentry into the earth's atmosphere, the injection rate could reach up to 13% [3]. Ahn H-K studied Pioneer-Venus, and the numerical simulations showed that during the entered into Venus atmosphere, when thermal blockage was taken into account, the level of heat flux decreased significantly by 55-60% of the net heat flux [4]. Since the last century, researchers has done a lot of research on wall injection. Kaattari G had studied the effects of wall injection on blunt-body boundary-layer transition and heat transfer in Ames 3.5-ft Hypersonic Wind Tunnel, and empirical heating rate data correlations were developed for the laminar and turbulent flow regimes [5]. Izawa Y and Sawada K developed a boundary condition for describing wall injection with normal velocity, and calculated the heat flux of a sphere with wall injection in hypersonic flow field [6].

As mentioned above, wall injection has an important influence on the aerodynamic heating environment in hypersonic flow, and wall injection are widely used in ablation chemical reactions of high-speed aircraft. Therefore, the numerical investigations of the influence of ablation chemical reactions considering wall injection on the aerodynamic heating environment are indispensable. There are interactions between aerodynamic heating environment and structural response of high-speed aircrafts, which leads to complex gas-solid coupling thermal effect, especially the high-temperature real-gas effects of gas-solid chemical reacting interface at high Mach number. Gas-solid coupling thermal effect and interface high-temperature real-gas effects have important influence on the effective prediction of aerodynamic heating environment of high-speed aircrafts, especially the interactions between ablation and aerodynamic heating environment. Therefore, when studying wall injection effect caused by ablation and the influence of wall injection effect on aerodynamic heating environment, it is urgent to study the coupling model of aerodynamic heating and structural thermal response under high-temperature real-gas effects. At present, some researches had considered the gas-solid coupling numerical calculation including ablation chemical reactions and interface high-temperature real-gas effects, which made the prediction of the aerodynamic heating environment of high-speed aircraft more accurate [7-10]. It is also important to study the influences of ablation chemical reactions on aerodynamic heating environment under different conditions and the heat transfer characteristics of ablation chemical reactions.

In this paper, the wall injection boundary condition was implemented in the in-house CAPTER code. After verifying the boundary condition, it was applied to the coupling modeling of chemically reacting interface. Then, based on the coupled model in CAPTER, the numerical simulations of the blunt leading edge model with wall injection due to ablation in hypersonic chemical nonequilibrium flow were carried out.

2. Methodology

2.1 CAPTER

The research of this paper was based on the in-house CAPTER (Coupled Analysis Platform for Thermal Environment and structure Response) developed by the aircraft thermal science group of China Aerodynamics Research and Development Center (CARDC) [11]. The platform includes calculation modules for numerical solution of hypersonic non-equilibrium flow, structural thermal response and interface physical and chemical effects. It has been verified by a large number of aerodynamic / structural coupling examples [11-14] and has strong engineering applicability.

2.2 Wall Injection Boundary Condition

In order to study the wall injection caused by ablation, the wall injection boundary condition was implemented in the in-house CAPTER code. The key point of the wall injection boundary condition is that, based on the viscous wall boundary condition, the conservation of momentum equation is used between the wall grid points and the first layer grid points adjacent to the wall to characterize the wall injection. For the wall injection boundary condition, the pressure gradient between the wall grid point and the first layer grid points adjacent to the wall is no longer equal to zero.

First, the direction is specified, where $\boldsymbol{n}$ is the identity vector normal to gas-solid interface, $\boldsymbol{\tau}$ and $\boldsymbol{\varepsilon}$ are the two identity vectors on the section to gas-solid interface. When we don't take into account the losses, the conservation of momentum equation between the wall grid points and the first layer grid points adjacent to the wall can be written as

$$P_{nw} + \rho_{nw} v_{\boldsymbol{n},nw}^2 = P_w + \rho_w v_{\boldsymbol{n},w}^2 \tag{1}$$

The wall injection mass flow rate at the wall can be expressed as

$$\dot{m}_{\boldsymbol{n},w} = \rho_w v_{\boldsymbol{n},w} \tag{2}$$

The ideal gas law can be written as

$$P_w = R_g \rho_w T_w \tag{3}$$

Similar to the viscous wall boundary condition, the velocity components in the non-vertical wall directions are zero, as

$$v_{\boldsymbol{\tau},w} = 0 \ , \ v_{\boldsymbol{\varepsilon},w} = 0 \tag{4}$$

Through the above five equations, all the required values at the wall can be obtained for further calculation. This boundary condition has been implemented in CAPTER code. Figure 1 shows the calculation process of the wall injection boundary condition in CAPTER code. Similar progress has been reported by Martinelli, et al. and Richard A. Thompson, et al. for other CFD codes [9,15].

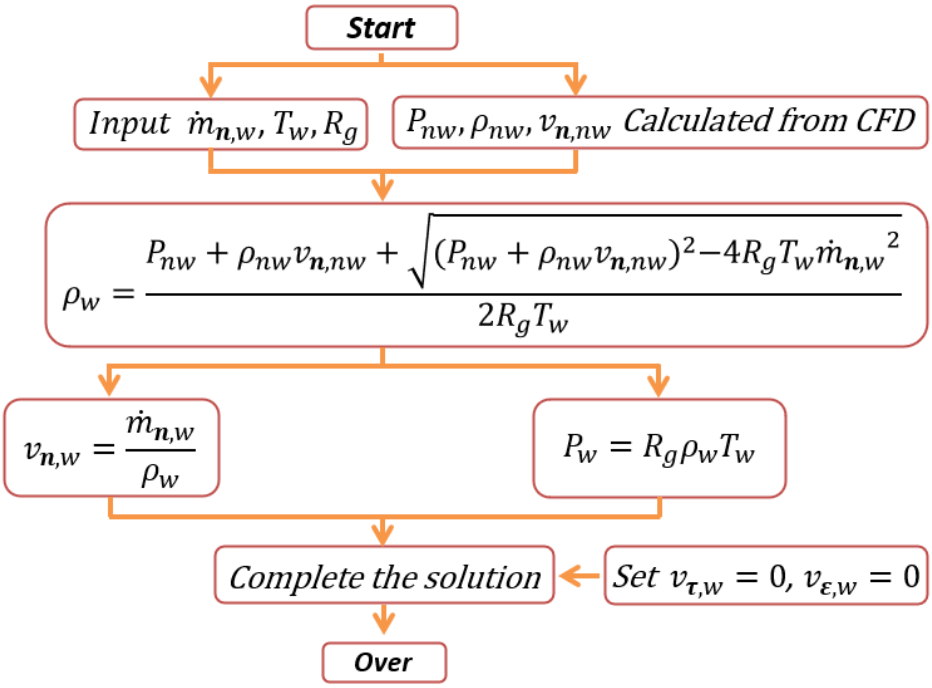

Figure 1 - The calculation process of the wall injection boundary condition in CAPTER.

In order to ensure the accuracy of wall injection boundary condition, the boundary condition was validated and evaluated. Marvin, J. G. et al. carried out an experimental study in Ames 3.5-ft Hypersonic Wind Tunnel [16] and theoretical calculations under the same conditions using the nonsimilar laminar boundary-layer equations including foreign gas Injection [17]. In this paper, the wall injection boundary condition based on CAPTER was used to calculate the problem numerically and the results were compared and evaluated. the calculation model is a 5° half-angle cone with impermeable tip and the porous surface. The impermeable tip region was set as the viscous wall boundary condition, and the porous surface region was set as the wall injection boundary condition. Corresponding to the experimental and theoretical calculation, the numerical calculation examples and parameters were set as shown in Table 1.

Parameter	Example1	Example2	Example3
Ma_∞	7.40		
$P_\infty(Pa)$	700.88		
$T_\infty(K)$	69.72		
$\rho_\infty(kg/m^3)$	0.035		
$T_w(K)$	300.00		
$\dot{m}_w/\dot{m}_\infty$	0.00%	0.04%	0.08%
$\dot{m}_w(kg/(m^2 \cdot s))$	0.00	0.018	0.035

Table 1 – Numerical calculation examples and parameters

Figure 2 shows the comparisons of the dimensionless heat flux calculated based on the wall injection boundary condition of CAPTER with the experimental data and theoretical calculation results at different wall injection mass flow rates. In this figure, the abscissa is the dimensionless

distance along the surface of the cone s/L, where the reference length $L = 95mm$. The ordinate is the dimensionless heat flux, where the reference heat flux q/q_{ref} , where the reference heat flux is $q_{ref} = 16.581\,kW/m^2$. It can be observed from the results in the figure that the heat flux results are relatively consistent and the trend is the same.

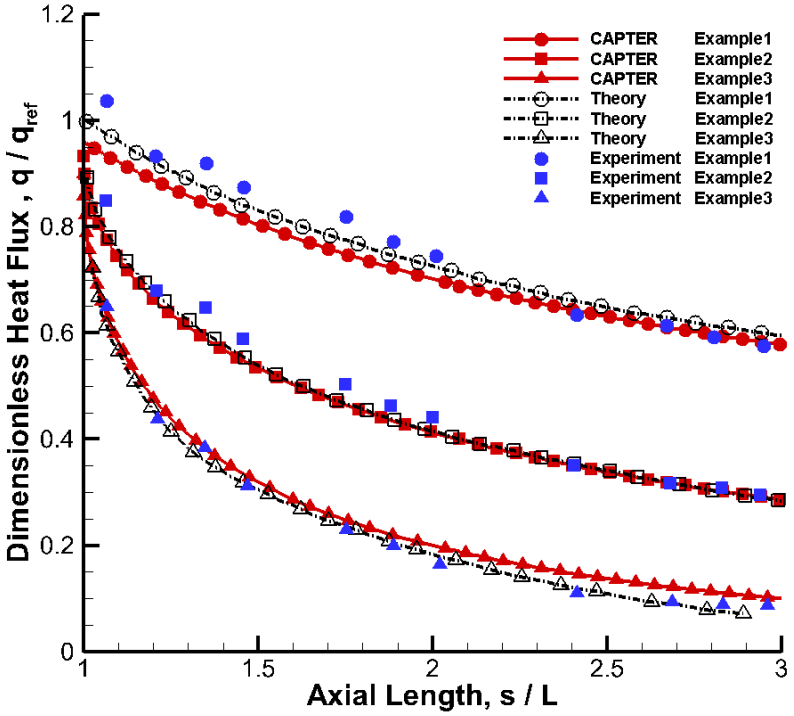

Figure 2 - The dimensionless heat flux results of the 5° half-angle cone

2.3 Coupling Simulation Solvers and Strategy

The coupling simulation solvers include CFD (Computational Fluid Dynamics) for high-enthalpy and chemical nonequilibrium flow, CHT (Computational Heat Transfer) for TPS structure heat transfer, and IB (Interface Balance) for describing gas-solid interaction and interface heat transfer behavior. Numerical method for flow solver and numerical method for structure temperature solver are consistent with those methods used by Yang et al [14]. The controlling equations on the gas-solid interface also follow the laws of conservation of mass, momentum and energy. After simplified expression as the interface balance equations [18], for steady state we have

$$\left(\dot{\mathbf{m}} - \rho \boldsymbol{Y}^{\mathrm{T}} \boldsymbol{u}\right) \cdot \boldsymbol{n} = \dot{\boldsymbol{m}}_{\mathrm{w,n}} \tag{5}$$

$$\nabla p \cdot \boldsymbol{n} = 0 \tag{6}$$

$$\left(\boldsymbol{q}_{\mathrm{g}} + \boldsymbol{h} \cdot \dot{\mathbf{m}}\right) \cdot \boldsymbol{n} = \boldsymbol{q}_{\mathrm{s}} \cdot \boldsymbol{n} + q_{\mathrm{w,r}} \tag{7}$$

where $\dot{\boldsymbol{m}}$ is mass flux matrix for all species in three directions, $\boldsymbol{Y}$ is mass fraction array for all species, $\boldsymbol{q}$ is heat flux array in three directions and $\boldsymbol{h}$ is enthalpy array for all species.

In view of the characteristic of gas injection caused by ablation, combined with the wall injection boundary condition, the momentum conservation equation on the interface balance equation was improved. The pressure gradient on the interface of the flow field was no longer zero, which is expressed as

$$P_{nw} + \rho_{nw} v_{\boldsymbol{n},nw}^2 = P_w + \rho_w v_{\boldsymbol{n},w}^2 \tag{8}$$

On the gas-solid interface, the net mass flow rate is determined by the interfacial reaction, and the relevant calculation method was consistent with that of Yang et al [14]. Among them, the ablation

reaction rate of the thermal protection materials involved in the wall chemical reaction depends on the wall temperature, ablation reation coefficient and ablation activation energy, the expression of the reaction rate

$$k_f = \left[\frac{\bar{v}}{4\Phi_{(b)}}\right]\gamma T'^{\beta}\exp(-\frac{E}{R_0 T}) \tag{9}$$

Where γ is the ablation reaction coefficient, β and E are the ablation temperature index and the activation energy of ablation reaction.

In this paper, we study the chemically reacting interface coupling considering wall injection. Physically and spatially, the whole system is decomposed into three modules: CFD, CHT and IB. We establish a coupling model, which connecting these three modules through appropriate coupling strategy. The relation of these three physical fields and their inter-field data transfer is presented in Figure 3.

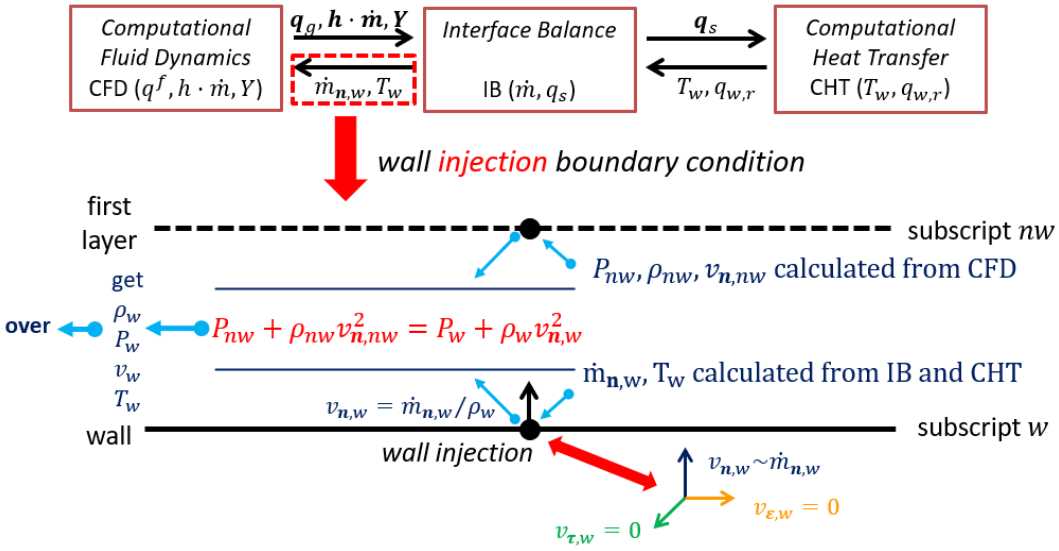

Figure 3 - The relation of three physical fields and their inter-field data transfer

3. Computation Models and Conditions

3.1 Geometry Model

As shown in Figure 4, the research object is a blunt leading edge ($R_n = 3mm$) of high-speed aircraft, which a solid structure made of Reinforced Carbon-Carbon (RCC) material. The three-dimensional hexahedral elements are used in the computational grids of flow field and structure field, while the two-dimensional quadrilateral elements are used in the computational grids of gas-solid interface, as shown in Figure 5. In order to simulate the details of boundary layer and heat flux more accurately, the flow field grids are properly densified and orthogonal enough (86.76°~93.24°) in the normal direction of the wall, and the Reynolds number of the first layer grids on the wall are in the order of O (1). The grids of structure field are also properly densified near the interface to better capture the process of temperature gradient.

Figure 4 - Geometry of the blunt leading edge

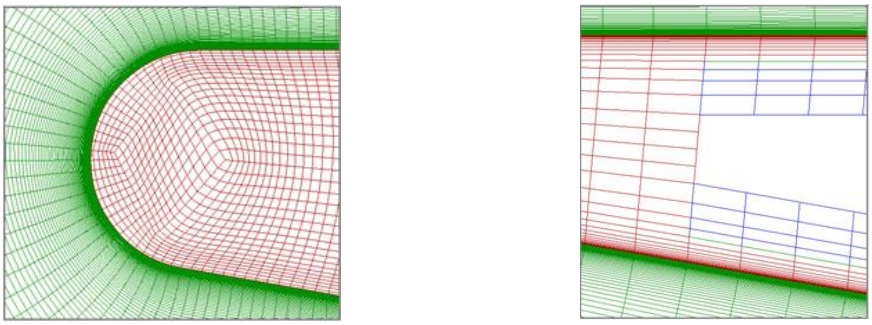

Figure 5 - The computational grids of Geometry of flow field, structure field and gas-solid interface

3.2 Reaction Models

For the high enthalpy dissociation of air mixture, the air dissociation model of 5 components (O, N, O2, N2 and NO) 34 chemical reactions established by Gupta [19] is adopted, and the molecular ionization is not considered. In addition, due to the oxidation of carbon on the surface of RCC material, there are additional 3 components (C, CO and CO2) 18 chemical reactions in the flow field [20].

In order to better research the wall injection caused by ablation, it is assumed that the wall is noncatalytic. For interface ablation, the gaseous oxygen atoms/molecules combine with the solid-phase carbon atoms on the surface of the RCC material. Two types of combination, A1 and A2, are involved as [21]

$$O + C(b) => CO + (b) \quad \text{A1}$$

$$O_2 + C(b) => CO + O + (b) \quad \text{A2}$$

where (b) denotes the bulk atom.

3.3 Computational Conditions

In the coupling calculation, the free stream conditions were set as follows: altitude 40 km, Mach number 15, zero angle of attack and zero sideslip angle. It was assumed that the aircraft at a given altitude and speed. The initial temperature of the aircraft was 300K. In this paper, the ablation chemically reactions and ablation reaction coefficients were changed to study their effects on wall injection, aerodynamic heating environment and flow field. Among them, the ablation chemical reactions included A1, A2 and their combination. The ablation reaction coefficients were set as 10^{-3}, 10^{-2}, 10^{-1} and 1.

4. Coupling Results and Discussion

Figure 6 shows that the temperature contour in the gas and solid domains under the above methods and conditions at the coupling time of 1 s. It can be clearly seen from Figure 7 that when the ablation reaction A1 is considered, the CO and streamline distribution in the flow field, the product CO of ablation reaction A1 injects from the wall and a film is formed near the wall.

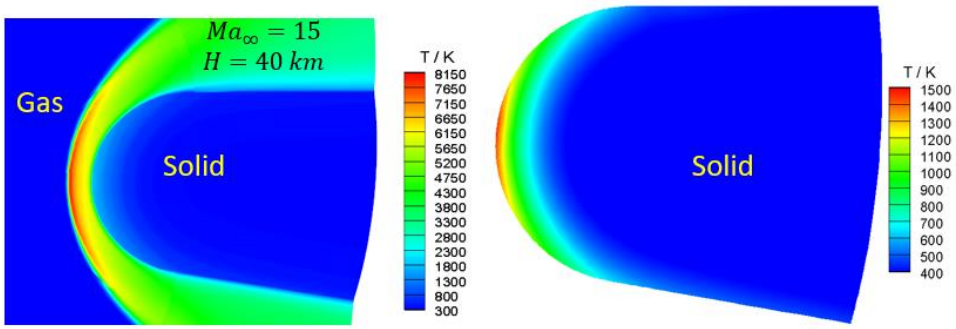

Figure 6 - Temperature contour in the gas and solid domains under the above methods and conditions at the coupling time of 0.1 s

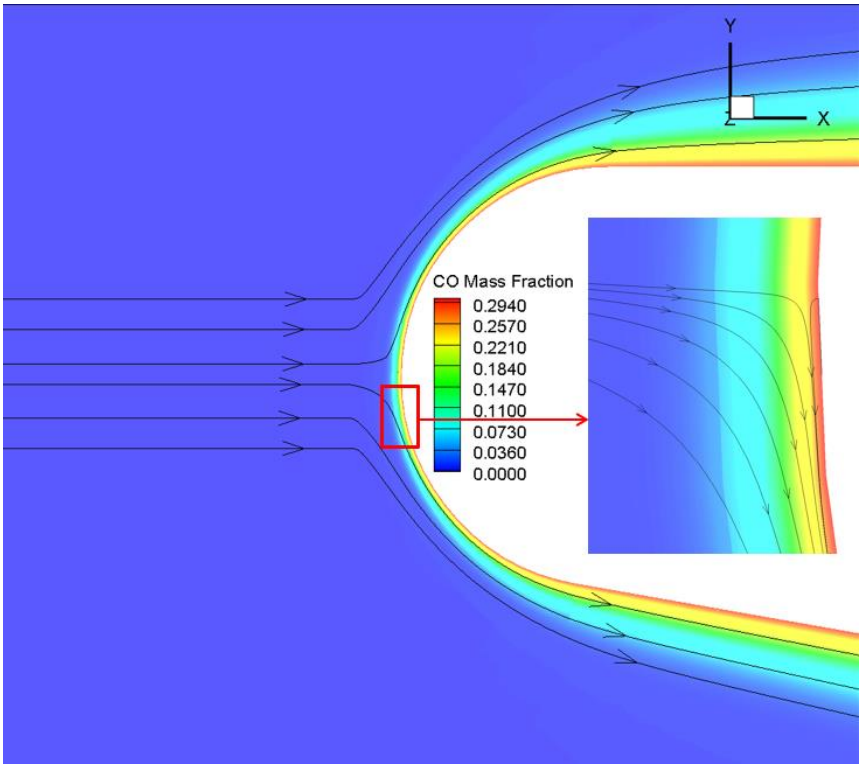

Figure 7 - CO and streamline distribution in the flow field

Figure 8 shows the stagnation heat flux results when only reaction A1, only reaction A2 and both reactions A1 and A2 are considered when the ablation reaction coefficient is 10^{θ} (θ= -3, -2, -1, 0). The results show that the stagnation heat flux of the case considering reaction A1 increases rapidly with the increase of ablation reaction coefficient, and the stagnation heat flux of the case considering reaction A2 decrease with the increase of ablation reaction coefficient, but have little influence on the aerodynamic thermal environment. The results show that with the increase of ablation reaction coefficient, the effect of ablation reaction on stagnation heat flux increases gradually, and the influence of A1 reaction on stagnation l heat flux is greater than that of A2 reaction. For the case of considering both A1 and A2 reactions, when the ablation coefficient is small, the results of stagnation heat flux are consistent with those of the cases considering only A1 reaction and A2 reaction, but with the increase of ablation coefficient, the results of stagnation heat flux of the case considering both A1 and A2 reactions are consistent with those of the case considering only A1 reaction.

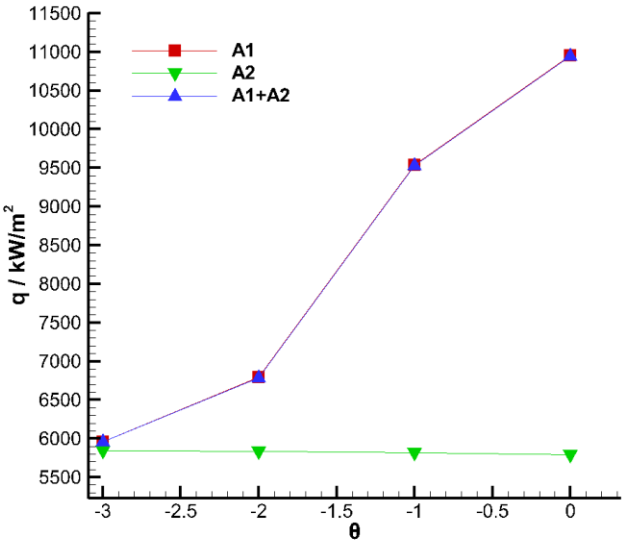

Figure 8 - Stagnation heat flux of coupling calculation

Figure 9 shows stagnation temperature and wall injection mass flow rate of the cases considering A1 reaction, A2 reaction and both A1 and A2 reactions under different ablation reaction coefficients. According to the ablation reaction rate expression (9), the ablation reaction rate is related to the material temperature and ablation reaction coefficient, and the ablation reaction rate determines the wall injection mass flow rate. From the results, we can find that the case considering reaction A1 material temperature increases with the increase of the ablation reaction coefficient, and the ablation reaction coefficient and the material temperature affect the mass flow rate together. Compared with the results of the case considering A1 reaction, the results of the case considering A2 reaction are almost negligible. When we separately observe the results of the case considering A2 reaction (as shown in the right figure of Figure 9), we can see that the material temperature decreases with the increase of ablation reaction rate, while the mass flow rate increases with the increase of ablation reaction coefficient. This is because A2 reaction is more intense with the increase of ablation reaction coefficient, and because A2 reaction is endothermic reaction, its mass flow rate increases and its temperature decreases. It is worth noting that from the calculation results, we can observe that under the conditions of this case, the influence of A2 reaction is much weaker than that of A1 reaction. For this reason, the temperature rises and mass flow rate increases of the case considering both A1 and A2 reactions are similar to that of the case considering A1, but the temperature is slightly lower than that of A1 and the mass flow rate is slightly higher than that of the case considering A1 due to the influence of A2 reaction.

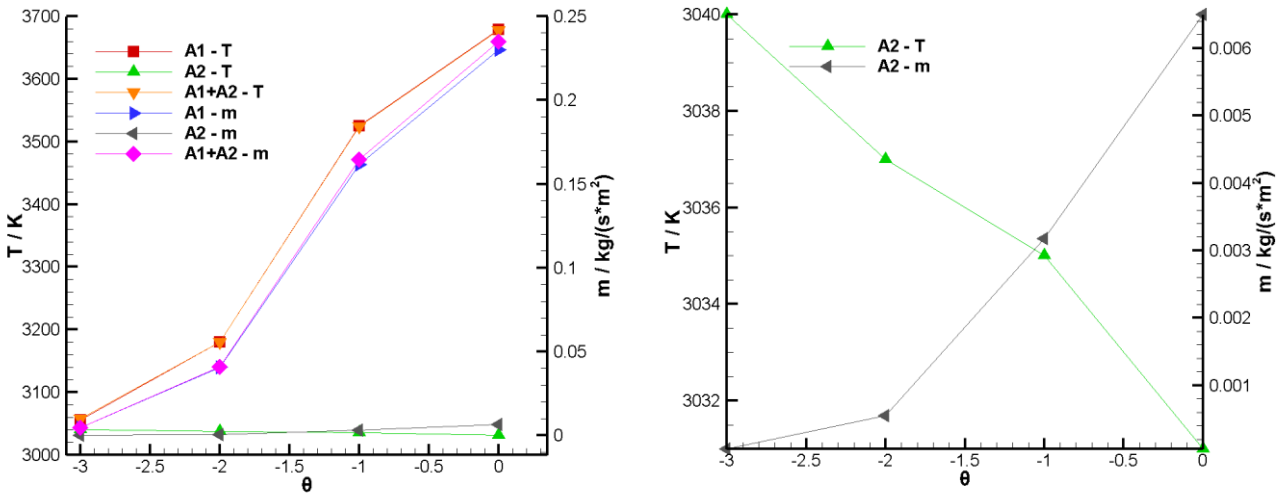

Figure 9 - Stagnation temperature and wall injection mass flow rate of the cases considering A1 reaction, A2 reaction and both A1 and A2 reactions under different ablation reaction coefficients

After the above analysis of the results, we found that under the same calculation conditions, A2 reaction is much weaker than A1 reaction. The reason is explored by analyzing the mass fraction of each component on the wall. As shown in Figure 10, the results of the mass fraction of each component on the wall are obtained respectively when there is no ablation reaction and when both A1 and A2 reactions are considered. It can be seen from the figure that the mass fraction of oxygen atom on the wall is much larger than that of oxygen molecule in the case of no ablation reaction. Similar results are obtained in the case of considering both A1 and A2 reactions, because the reactant of A1 reaction is oxygen atom and the reactant of A2 reaction is oxygen molecule, which results in that A1 reaction is more intense than A2 reaction under this condition, Moreover, the product of A2 contains oxygen atoms, which can promote the A1 reaction. In addition, we can also see that when there is no ablation, there is no carbon monoxide formation, so its mass fraction is zero. When both A1 and A2 reactions are considered, there is carbon monoxide formation on the wall, and the ablation at stagnation point is the most serious, so the mass fraction at stagnation point is the largest and then decreases gradually.

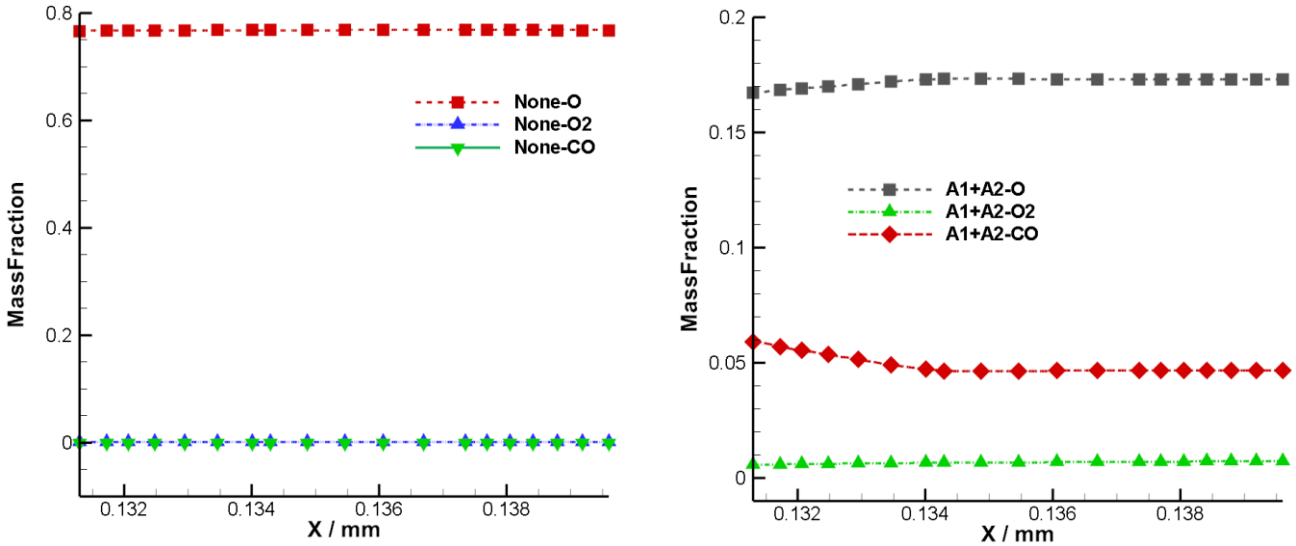

Figure 10 - Mass fraction results of each component on the wall of the cases without ablation and considering both A1 and A2 reactions

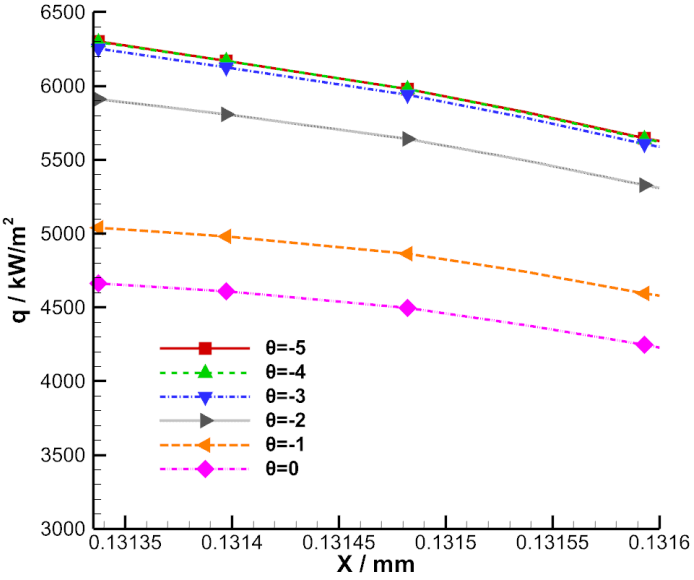

Figure 11 - Heat flux caused by convective heat transfer results of the case considering A1 reaction under different ablation reaction coefficients

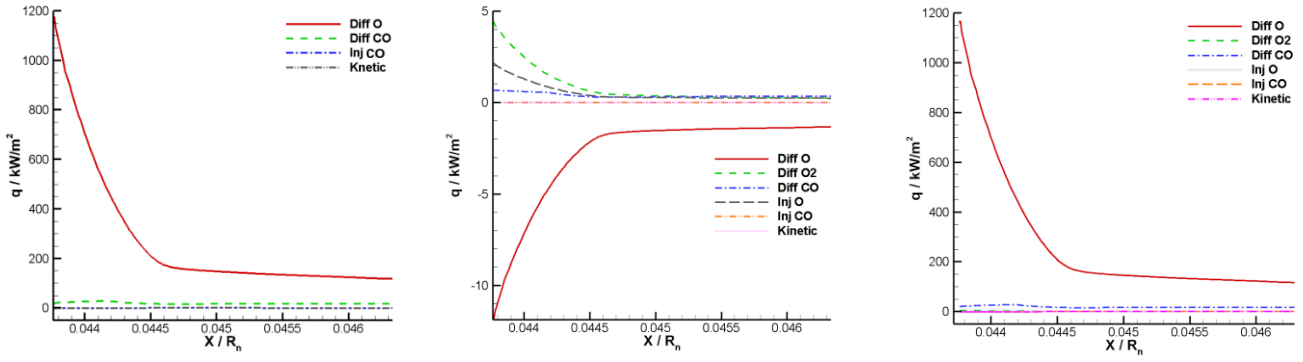

Figure 12 - Heat transfer characteristics of A1 reaction, A2 reaction and both A1 and A2 reactions

The previous results show that with the increase of ablation reaction coefficient, the wall injection mass flow rate of A1 reaction, A2 reaction and both A1 and A2 reactions increase. Previous

studies have shown that the wall injection has a significant effect on the aerodynamic heating environment [3]. The wall injection mainly affects the convective heat transfer. Figure11 shows the results of heat flux caused by convective heat transfer near stagnation point under different ablation coefficients in the case of A1 reaction. It can be observed that the heat flux decreases with the increase of ablation reaction coefficient. In addition, ablation also affects the aerodynamic heating environment through gas diffusion, the energy of injected gas and the momentum carried by injected gas. Figure 12 shows the heat transfer characteristics of the cases considering A1 reaction, A2 reaction and both A1 and A2 reactions. It can be seen that the diffusion of O plays a leading role in the aerodynamic heating environment, and the energy carried by the injected gas and the kinetic energy of the injected gas have little effect on the aerodynamic heating environment.

5. Conclusion

In this paper, the wall injection boundary condition was implemented in the CAPTER code. After verifying the boundary condition, it was applied to the coupling modeling of chemically reacting interface. Then, based on the coupled model in CAPTER, the numerical simulations of the blunt leading edge model with wall injection due to ablation in hypersonic chemical nonequilibrium flow were carried out. The effects of different ablation reactions and different ablation reaction coefficients on aerodynamic heating environment and flow field were investigated.

Through the analysis of the results, we found that the ablation reaction coefficient has a significant effect on the ablation intensity, and then affects the aerodynamic heating environment and wall injection effect. Different ablation reactions have different reaction mechanisms, and different reaction superposition calculations produce comprehensive effects and influence each other. It is found that the convective heat transfer is affected by the ablation reaction coefficient, and the diffusion heat transfer has a great influence on the aerodynamic thermal environment besides the convective heat transfer.

6. Acknowledgment

The authors gratefully acknowledge the financial support of the National Key Research and Development Program of China through the project No. 2019YFA0405202.

7. Contact Author Email Address

Associate Prof. Dr. Lei Zeng, China Aerodynamics Research and Development Center, Mailto: zenglei0ok@126.com

8. Copyright Statement

References

[1] Gui Y, Tang W and Du Y. *Thermal safety issues of near-space hypersonic vehicles*. 1st edition, National Defense Industry Press, 2019.

[2] Guo Y, Shi W and Zeng L. *Mechanism of ablative thermal protection applied to hypersonic vehicles*. 1st edition, Science Press, 2019.

[3] Reynier P. Survey of convective blockage for planetary entries. *Acta Astronautica*, Vol. 83, pp 175-195, 2013.

[4] Ahn H-K, Park C and Sawada K. Dynamics of pyrolysis gas in charring materials ablation. *36th AIAA Aerospace Sciences Meeting and Exhibit*, Reno, AIAA Paper 98-0165, 1998.

[5] Kaattari G. Effects of mass addition on blunt-body boundary-layer transition and heat transfer. NASA TP-1193, 1978.

[6] Izawa Y and Sawada K. Calculation of surface heat transfer for a sphere with wall injection. *JOURNAL OF*

THERMOPHYSICS AND HEAT TRANSFER, Vol. 14, No. 2, pp 230-236, 2000.

[7] Olynick D, Chen Y-K and Tauber M E. Aerothermodynamics of the stardust sample return capsule. *Journal of Spacecraft and Rockets*, Vol. 36, No.3, pp 442-462, 1999.

[8] Suzuki K, Kubota H and Fujita K. Chemical nonequilibrium ablation analysis of MUSES-C super-orbital reentry capsule. *32nd Thermophysics Conference*, Kanagawa, AIAA Paper 97-2481, 1997.

[9] Thompson R A and Gnoffo P A. Implementation of a blowing boundary condition in the LAURA code. *46th AIAA Aerospace Sciences Meeting and Exhibit*, Reno, AIAA Paper 2008-1243, 2008.

[10] Farbar E, Alkandry H and Wiebenga J. Simulation of ablating hypersonic vehicles with finite-rate surface chemistry. *AIAA AVIATION 2014 -11th AIAA/ASME Joint Thermophysics and Heat Transfer Conference*, Atlanta, AIAA Paper 2014-2124, 2014.

[11] Gui Y, Liu L and Dai G. Research status of hypersonic vehicle fluid-thermal-solid coupling and software development. *Acta Aeronautica ET Astronautica Sinica*, Vol. 38, No. 7, 020844, 2017.

[12] Yang X, Gui Y and Tang W. Surface thermochemical effects on TPS-coupled aerothermodynamics in hypersonic Martian gas flow. *Acta Astronautica*, Vol. 147, pp 445-453, 2018.

[13] Yang X, Gui Y and Liu L. Influence of surface catalysis on coupled aerodynamic heating for Mars entries. *Scientia Sinica Technologica*, Vol. 48, No.9, pp 939-949, 2018.

[14] Yang X, Du Y and Liu S. Coupled heat transfer characteristics on gas-solid reacting interface in carbon-oxygen dissociating environment for spacecraft entry flow. *Journal of Thermal Science and Technology*, Vol. 15, No. 2, pp1-21, 2020.

[15] Martinelli S, Ruffin S and McDaniel R. Validation process for blowing and transpiration-cooling in DPLR. *39th AIAA Thermophysics Conference*, Miami, AIAA Paper 2007-4255, 2007.

[16] Marvin J G and Akin C M. Combined effects of mass addition and nose bluntness on boundary-layer transition. *AIAA Journal*, Vol. 8, No. 5, pp 857-863, 1970.

[17] Marvin J G and Sheaffer Y S. A method for solving the nonsimilar laminar boundary-layer equations including foreign gas injection. NASA TN D-5516, 1969.

[18] Milos F S and Rasky D J. Review of numerical procedures for computational surface thermochemistry. *Journal of Thermophysics and Heat Transfer*, Vol. 8, No. 1, pp 24-34, 1994.

[19] Gupta R N, Yos J M and Thompson R A. A review of reaction rates and thermodynamic and transport properties for an 11-species air model for chemical and thermal nonequilibrium calculations to 30000 K, NASA Reference Publication, 1990.

[20] Park C, Howe J T and Jaffe R L. Review of chemical-kinetic problems of future NASA missions, II: Mars entries, *Journal of Thermophysics and Heat Transfer*, Vol. 8, No. 1, pp 9-23, 1994.

[21] Keenan J A and Candler G V. Simulation of graphite sublimation and oxidation under re-entry conditions, AIAA/ASME 6th Joint Thermophysics and Heat Transfer Conference, AIAA Paper 94-2083, 1994.